Matter

CellPress

Article

Continuously growing multi-layered hydrogel structures with seamless interlocked interface

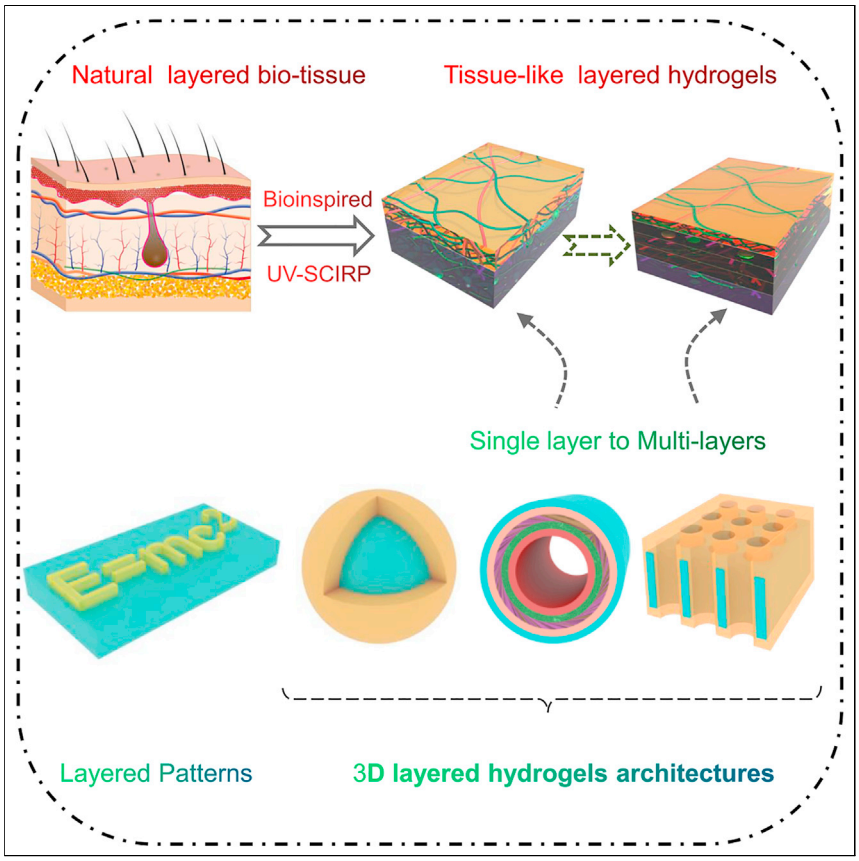

Herein, a method, namely, ultraviolet-triggered surface catalytically initiated radical polymerization (UV-SCIRP), is reported for preparing layered structural hydrogels with a living polymerization growing process resembling the growth route of natural bio-tissues, in which Fe^{2+} ions were generated *in situ* from the surface-bound Fe^{3+} ions of a hydrogel substrate to catalyze radical polymerization at the solid-liquid interface to grow hydrogel layers at room temperature. The versatile method is effective in constructing complex hydrogel patterns and arbitrarily shaped layered hydrogel architectures.

Rongnian Xu, Mutian Hua, Shuwang Wu, ..., Meirong Cai, Ximin He, Feng Zhou

mashuanhong@licp.cas.cn (S.M.)
ximinhe@ucla.edu (X.H.)
zhouf@licp.cas.cn (F.Z.)

Highlights

UV-SCIRP method imitates the time-dominated living growth process of bio-tissues

The hydrogel layer number is unlimited and the layer interface is seamless and robust

Suitable for making layered hydrogel architecture with arbitrary shape and size

Enables selective growth and patterned precision construction of hydrogel layers

Development
Practical, real world, technological considerations and constraints

Xu et al., Matter 5, 634–653
February 2, 2022
https://doi.org/10.1016/j.matt.2021.11.018

CellPress

Matter

Article

Continuously growing multi-layered hydrogel structures with seamless interlocked interface

Rongnian Xu,[1,2] Mutian Hua,[3] Shuwang Wu,[3] Shuanhong Ma,[1,4,*] Yunlei Zhang,[1,2] Liqiang Zhang,[1,2] Bo Yu,[1] Meirong Cai,[1] Ximin He,[3,*] and Feng Zhou[1,*]

SUMMARY

Many natural tissues feature layered structures for multi-functionality as each layer consists of different cell types and therefore exhibits unique physicochemical properties. Creating such complex multi-layered structures in human-made soft materials is hardly achievable with common gelation methods, lacking spatiotemporal control, and thus demands a living polymerization-based controllable continuous growing process to imitate bio-tissue growth. Herein, a method, namely, ultraviolet-triggered surface catalytically initiated radical polymerization (UV-SCIRP), is demonstrated in living growth of uniform hydrogel layers at room temperature, facilitated by the *in situ* generation of Fe^{2+} ion catalysts from the surface-bound Fe^{3+} ions of the hydrogel substrate. Reiterative application of UV-SCIRP enables fabrication of multi-layered hydrogels with diverse components and layered features. The surface-catalyzed gelation makes the method effective in constructing complex hydrogel patterns, non-flat arbitrary-shaped hydrogel objects, and blood vessel-like intricate multi-layered hydrogel tubes. This work manifests a new route to engineer bioinspired structural hydrogels and complex soft architectures with on-demand functions.

INTRODUCTION

Hydrogels have garnered extensive attention in the broad fields of biomedicine, soft robotics, and wearable devices,[1–5] owing to the close resemblance of their structural and biochemical properties to those of natural bio-tissues. The fact that the features of the typical layered structures exhibited by natural bio-tissues,[6,7] including skin,[8] tendon,[9] blood vessel,[10] articular cartilage,[11] and muscle,[12] confer living organisms with certain intricate functions necessitates the innovation of facile methods for fabricating biomimetic structural hydrogels with controllable geometries and sizes, to fulfill broad awaiting applications. In nature, each layer of bio-tissue has different cell types that provide specific physical or chemical properties (i.e., high toughness, high diffusivity, or low friction). Correspondingly, formation of those layered bio-tissues is always a time-dominated, living growing process, for which the micronetwork structure, geometric size, thickness, components, and mechanical property of the layer can be finely controlled. Therefore, among all the aspects of structural hydrogels, incorporating a layered feature in these objects is of tremendous interest, due to its ample applications in the fields of biomedicine,[13–15] actuation,[16–19] lubrication,[20,21] and tissue engineering[22,23] as tissue-like organs, soft robots, and flexible wearable devices. The past couple of decades have witnessed significant advances pertaining to the fabrication of diverse layered hydrogels. So far, a number of fabricating technologies for layered hydrogels that provide structural functions more analogous to natural tissues have been

Progress and potential

Constructing structural hydrogels with layered, anisotropic, and hierarchical structures has attracted interest because of their bio-tissue-like properties. Current classic preparation techniques for layered hydrogels are typically physical manufacturing routes, like mechanically building a wall by continuously stacking bricks. In this work, a novel method, named ultraviolet-triggered surface catalytically initiated radical polymerization (UV-SCIRP), is reported for preparing layered structural hydrogels with a living polymerization growing process, which resembles the growth of natural bio-tissues. The fabrication of diverse multi-layered hydrogel materials with tunable layer thickness, composition, geometry, and size is achievable by UV-SCIRP. This original strategy provides a route for developing bioinspired layered hydrogel structures for a wide range of applications, including tissue-like manufacture, biomedicine carrier, intelligent robotics, and functional soft devices.

developed, including self-assembly (SA),[4,24–29] separated spatial patterns mechanism,[30] stepwise technique,[31–34] photo-polymerization,[35–38] sequential electro-spinning,[39–41] 3D printing,[42] double-hydrophobic-coating method,[43] and so on.[44,45]

In the aforementioned methods for designing layered structural hydrogel materials, typically the preparation process is a physical-stacking manufacturing route, like mechanically building a wall by continuously stacking bricks. For each layer, in order to obtain a fixed thickness, one must design chemical components of materials and manufacture parameters of equipment in advance. Correspondingly, the total thickness or property of the resultant layered hydrogels is related only to the number of bricks and cannot be precisely controlled by dynamic time evolution. Therefore, construction of layered hydrogels by imitating a time-dominated living growth process of natural bio-tissue is still difficult. Zarket and Raghavan[46] first suggested a novel chemical strategy to construct onion-like layered hydrogel capsules by following the growth manner of natural materials, based on an initiator diffusion-dominated polymerization reaction mechanism. Despite a huge breakthrough, this reported method needs to preload a high-concentration initiator (15 mg/mL) within the new-formed bulk hydrogel network shell and then add extra accelerator/viscosity modifier in monomer solution, which inevitably complicates the preparation process and increases the risk of unwanted polymerization of monomer solution along with initiator diffusion. Therefore, it is still extremely challenging to develop a new and generalizable chemistry methodology to fulfill the demand of continuous and controllable preparation of multi-layered hydrogels to vividly simulate the living growth process of layered biological tissue.

Yet, current common gelation methods for layered design can hardly precisely control the network features (microstructure, composition, and mechanical properties) of each layer, the total thickness, and the layer numbers, let alone accommodate complex geometric structures and a wide range of sizes. Essentially, the key to breaking the aforementioned bottleneck lies in achieving effective spatial confinement and temporal triggering of the polymerization reaction, such that the reaction occurs only at the solid-liquid interface exposed to the triggering signal. Analogs to the controlled polymerization methods include the classic surface-initiated atom transfer radical polymerization (SI-ATRP), which opened up unlimited opportunities with its unprecedented controllability of polymer-chain living growth on substrate surface.[47,48] If such a high-level spatiotemporal controllability of gel network living growth could also be achieved, it would make an important and impactful contribution to surface gelation methods and broad hydrogel fields, enabling previously unachievable technologies for tissue engineering, coatings for medical instruments, soft robotics, wearable devices, and human-machine interfaces.

Herein, adopting the redox mechanism of reducing Fe^{3+} ions into Fe^{2+} ions in the presence of UV irradiation and citrate acid,[49,50] we propose generating Fe^{2+} catalysts *in situ* on the surface of Fe^{3+}-loaded hydrogel substrate via controlled UV exposure, which then induces the catalytic decomposition of potassium persulfate into sulfate radicals, thus initiating the real-time radical polymerization of monomer solution for generating a new thin layer of hydrogel at the solid-liquid interface by adopting our previous surface catalytically initiated radical polymerization mechanism.[51] The proposed method is defined as the UV-triggered surface catalytically initiated radical polymerization (UV-SCIRP), in which polymerization can be mildly performed at room temperature in a normal monomer solution without any accelerator/modifier. Compared with common gelation methods for layered design, UV-SCIRP features good spatiotemporal control of the gel network living

[1]State Key Laboratory of Solid Lubrication, Lanzhou Institute of Chemical Physics, Chinese Academy of Sciences, Lanzhou 730000, China

[2]Center of Materials Science and Optoelectronics Engineering, University of Chinese Academy of Sciences, Beijing 100049, China

[3]Department of Material Science and Engineering, University of California Los Angeles, Los Angeles, CA 90095, USA

[4]Lead contact

*Correspondence: mashuanhong@licp.cas.cn (S.M.), ximinhe@ucla.edu (X.H.), zhouf@licp.cas.cn (F.Z.)

https://doi.org/10.1016/j.matt.2021.11.018

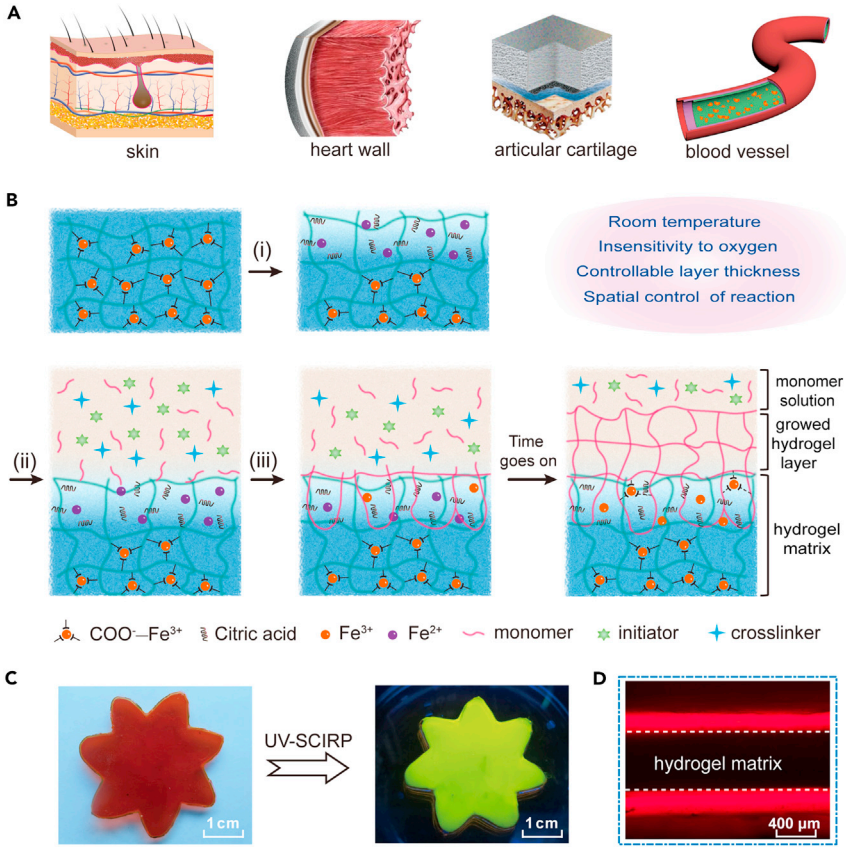

Figure 1. Concept display and schematic diagram of UV-SCIRP method

(A) Schematic diagrams of natural bio-tissues, including skin, heart wall, articular cartilage, and blood vessel.

(B) A schematic illustration of the preparation process of layered structural hydrogel materials through the UV-SCIRP method: (i) *in situ* generation of Fe^{2+} ion catalysts on the surface of the Fe^{3+}-loaded hydrogel substrate, triggered by citrate acid under UV irradiation; (ii) immersing the surface-activated (containing Fe^{2+} ions) hydrogel substrate (green network) in the monomer solution to perform interface polymerization; (iii) interpenetrating hydrogel layer (red network) begins to form at the solid-liquid interface; and (time goes on) robust hydrogel coating forms on the surface of the hydrogel substrate while the surrounding monomer solution remains non-polymerized.

(C) A photograph of the flower-like $H_{PAA\text{-}PAM/Fe3+}$ substrate and its subsequent fluorescence image (dyed with 1 mg/mL rhodamine 6G) after growing an $H_{PAA\text{-}PAM}$ coating by the UV-SCIRP method.

(D) A cross-sectional fluorescence microscope image of the flower-like $H_{PAA\text{-}PAM/Fe3+}$ after growing the $H_{PAA\text{-}PAM}$ coating.

growth on a hydrogel surface and thus can create intricate hydrogel architectures previously unachievable by simple physical stacking. By repeating UV-SCIRP, we provide a universal strategy for the design and fabrication of diverse multi-layered hydrogel materials with tunable layer thickness, composition, geometry, and size based on a time-dominated living polymerization growing process.

RESULTS AND DISCUSSION

The process of UV-SCIRP

As shown in Figure 1A, a majority of the natural bio-tissues, including skin, heart wall, articular cartilage, and blood vessels, show apparent layered structure. The layered structure plays a very important role in the normal activities of living organisms,

which integrate multiple properties and functions in the same tissue. Using the proposed UV-SCIRP method, we could facilely fabricate layered structural hydrogels resembling natural bio-tissues. The method is based on the chemistry that an anion-enriched hydrogel can absorb Fe^{3+} ions and, upon UV radiation, the surface layer of Fe^{3+} ions is reduced to Fe^{2+} ions *in situ*, which further catalytically decompose the persulfate to generate free radicals, to induce monomer polymerization. The detailed preparation process is illustrated in Figure 1B. First, Fe^{2+} ions that act as catalysts were generated *in situ* on the surface of the Fe^{3+}-loaded hydrogel substrate after immersion in citric acid aqueous solution and subsequent UV irradiation (Figure 1B-i). The poly(acrylic acid)-poly(acrylamide)/Fe^{3+} (PAA-PAM/Fe^{3+}) hydrogel substrate was immersed in the citric acid aqueous solution with a controlled pH of 3.0, which allowed the simultaneous reaction between citric acid and PAA chains with Fe^{3+} ions, resulting in the partial coordination of Fe^{3+} ions with citric acid (Figure S1A). At the pH of 3.0, only one carboxyl group of citric acid underwent deprotonation; hence, the deprotonated carboxyl group coordinated with Fe^{3+} ions to form an Fe^{3+}-citric acid complex. Afterward, the above-treated hydrogel substrate was put into a customized transparent glass mold and exposed to UV radiation (365 nm, 15 mW/cm^2) with proper distance (to avoid hydrogel dehydration). As a result, the Fe^{3+} ions that coordinated with the citric acid were reduced to Fe^{2+} ions, while the citric acid tended to be decarboxylated after undergoing the UV-assisted photochemical reaction (Figure S1B).[52,53] Subsequently, the hydrogel substrate retaining a superficial layer of Fe^{2+} ion catalysts was immersed in the monomer solution containing vinyl monomer; an initiator, $(NH_4)_2S_2O_8$ (APS); and a cross-linker, N,N′-methylenebis (acrylamide) (MBAA), to carry out the interfacial radical polymerization (Figure 1B-ii). Because the Fe^{2+} ions are capable of rapidly reducing the decomposition activation energy of $S_2O_8^{2-}$ ions to generate SO_4^{-} at the chain-initiation step, the polymerization rate of vinyl monomer at the solid-liquid interface of the monomer solution and the hydrogel surface witnessed an apparent acceleration.[54] Consequently, the new hydrogel layer (red network in the figure) was gradually formed at the top surface of the original hydrogel substrate at room temperature, which interpenetrated with the substrate network to yield a seamless interface (Figure 1B-iii). With the extension of polymerization time, the thickness of the formed hydrogel layer gradually increased at the solid-liquid interface. Finally, a uniform hydrogel layer with controllable thickness was generated *in situ* on the surface of the original hydrogel substrate at room temperature with the time goes on, while the bulk solution was kept non-polymerized (Figure 1B). Hence, the resultant layered structural hydrogels created through the UV-SCIRP method embodied the original hydrogel substrate and its coating layer. The various as-prepared layered hydrogel materials pertaining to different hydrogel substrates and coating layers can be denoted as H_m (H refers to hydrogel; m refers to the composition of hydrogel). As shown in Figure 1C, the flower-like $H_{PAA\text{-}PAM/Fe3+}$ substrate turned fluorescent on dyeing it with 1 mg/mL rhodamine 6G after growing an $H_{PAA\text{-}PAM}$ layer as a hydrophilic coating. The generated $H_{PAA\text{-}PAM}$ coating was more distinctively observable through a cross-sectional fluorescence image (Figure 1D). As speculated, this presented method exhibits four remarkable advantages: reaction at room temperature, insensitivity to oxygen, controllable thickness, and spatial control of reaction. Thus, the UV-SCIRP method emerges as an effective and convenient fabrication technique for tissue-like layered hydrogel materials with robust interface bonding.

Reaction mechanism and polymerization kinetics

To visually show the time-dependent reduction of Fe^{3+}, xylenol orange (XO) was employed as an indicator for Fe^{3+} ions, and the color of its aqueous solution changed from red-purple to blue-purple after interacting with Fe^{3+} ions.[55] A series

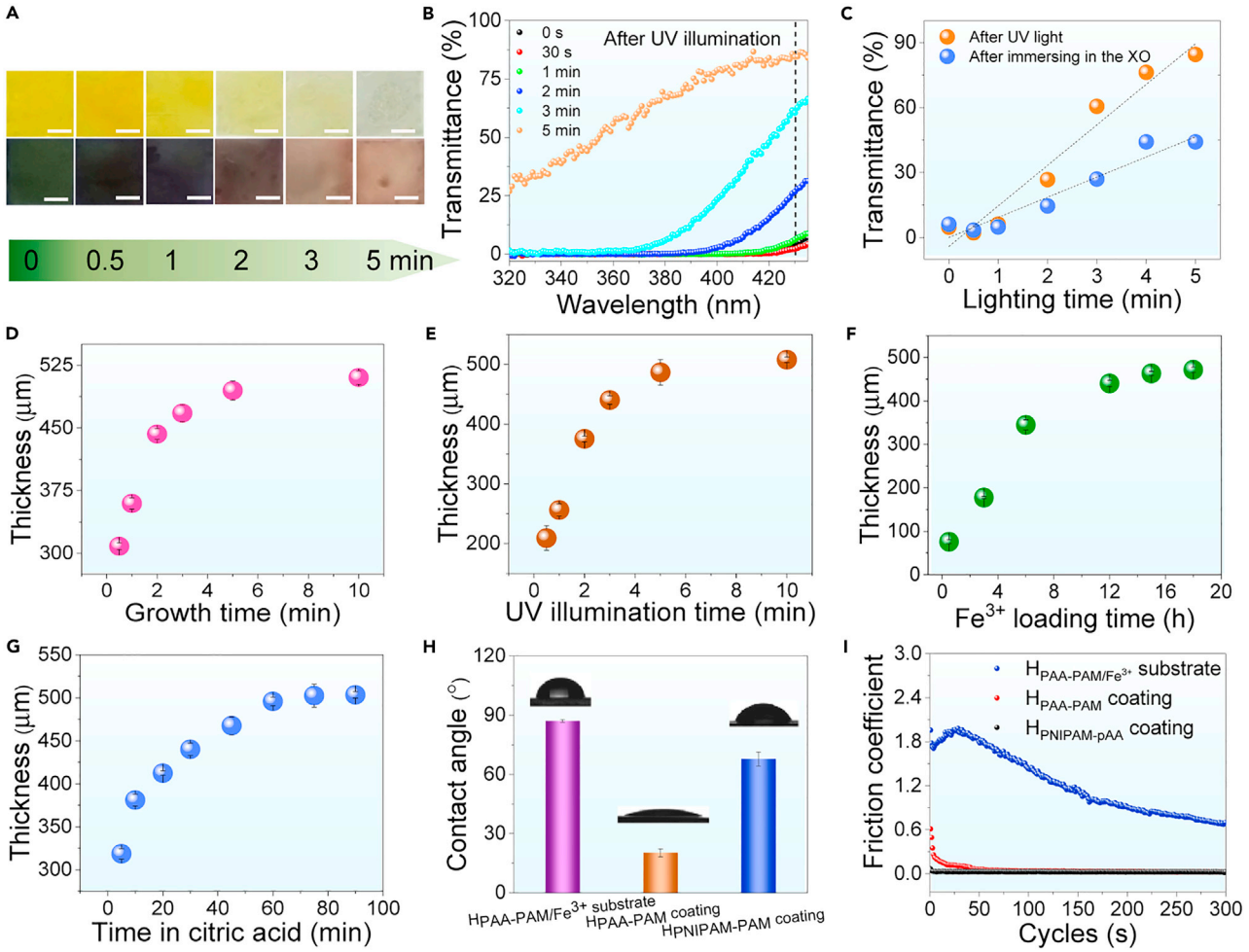

Figure 2. Mechanism characterization and polymerization kinetics

(A) Optical images of $H_{PAA\text{-}PAM/Fe3+}$ substrate after irradiating with UV light for different times (top) and subsequently immersing in the xylenol orange aqueous solution (0.01 mg/mL) for 2 min (bottom) (scale bar, 5 mm).

(B) The transmittance curve of $H_{PAA\text{-}PAM/Fe3+}$ substrate after irradiating with UV light for different times for the samples in (A [top]).

(C) The corresponding transmittance obtained at 430 nm for samples in (A).

(D–G) The thickness changes of $H_{PAA\text{-}PAM}$ coating with growth time (D), UV illumination time (E), Fe^{3+} loading time (F), and treating time in citric acid (G) on the surface of $H_{PAA\text{-}PAM/Fe3+}$ substrate. The data in (D) and (E) are presented as mean ± SD and sample size n = 5.

(H) The static contact angle of water droplets on the surface of bare $H_{PAA\text{-}PAM/Fe3+}$ substrate, $H_{PAA\text{-}PAM}$ coating, and $H_{PNIPAM\text{-}PAA}$ coating. The data are presented as mean ± SD and sample size n = 3.

(I) The friction coefficient curves of bare $H_{PAA\text{-}PAM/Fe3+}$ substrate, $H_{PAA\text{-}PAM}$ coating, and $H_{PNIPAM\text{-}PAA}$ coating at 0.2 N load and 1 Hz frequency for sliding for 5 min (300 reciprocating cycles).

of $H_{PAA\text{-}PAM/Fe3+}$ substrate materials were subjected to different illumination times under the UV light and later used for analysis. The UV illumination time for the hydrogel materials was gradually increased from left to right (Figure 2A, top), resulting in an increasing number of Fe^{3+} ions reduced to Fe^{2+} ions and the gradual fading of the hydrogels' color until they became colorless. Correspondingly, the color of these hydrogel materials varied from blue-purple to red-purple (Figure 2A, bottom) after immersion in XO aqueous solution for 2 min, as a smaller number of Fe^{3+} ions were able to coordinate with XO to form the blue-purple colored complex. The significant color variation can be determinably characterized by monitoring the UV transmittance under a wide range of wavelength from 320 to 435 nm (Figures 2B and S2). Correspondingly, the transmittance obtained at 430 nm further aided in

verifying the above speculation (Figure 2C). Furthermore, the X-ray photoelectron spectroscopy (XPS) fine spectrum of Fe element obtained from the surface of the irradiated hydrogel materials shows the reasonable distinguishing of the two peaks found at 710 and 710.5 eV, further validating the proof of the reduction of half of the Fe^{3+} ions to Fe^{2+} ions (Figure S3). The adjustable amount of Fe^{2+} ions controlled by the UV illumination time can be further used to realize the tunable thickness of the generated hydrogel coating.

Here, $H_{PAA-PAM}$ coating was taken as an example to quantitatively evaluate several factors, including growth time, UV illumination time, Fe^{3+} loading time, and immersion time in citric acid. As shown in Figure 2D, the thickness of $H_{PAA-PAM}$ coating increased from 308 to 510 μm, with corresponding growth time from 30 s to 10 min. The growth rate curve in Figure S4 clearly shows that the growing process of $H_{PAA-PAM}$ coating is living. The growth rate changes over growth time. The optical microscope photographs revealed evident growth during the process (Figure S5). A positive correlation could also be found between the coating thickness and the UV illumination time (Figure 2E), due to the fact that the Fe^{2+} ions responsible for catalyzing the polymerization were formed under UV illumination. As shown in Figure 2F, the $H_{PAA-PAM}$ coating thickness also increased from 76 to 471 μm with an escalating Fe^{3+} loading time from 30 min to 18 h, since a longer duration of the Fe^{3+} loading time enables the generation of more Fe^{2+} ions to catalyze polymerization. Moreover, it was found that extending the immersion time from 5 to 90 min for the original hydrogel materials in citric acid could also effectively increase the $H_{PAA-PAM}$ coating thickness from 319 to 503 μm (Figure 2G), which could be credited to the longer coordination time between citric acid and Fe^{3+} ions that helped to produce more Fe^{2+} ions. All the above-mentioned results indicate that the polymerization kinetics offered by the UV-SCIRP method are controllably governed by the amount of Fe^{2+} ions on the superficial layer of the UV-irradiated substrate surface. As a comparison, bulk $H_{PAA-PAM}$ substrate loaded with Fe^{2+} ions was also prepared and then immersed into monomer solution for performing radical polymerization. Unfortunately, the monomer solution became polymerized completely only after 2 min because the bulk Fe^{2+} ion catalyst diffused quickly into monomer solution to initiate uncontrollable polymerization (Figure S6), indicating its uncontrollable reaction feature from ultrafast catalyst diffusion.

The compositions of hydrogel materials obtained before and after growing the $H_{PAA-PAM}$ coating were verified through Fourier transform infrared spectroscopy (FTIR). Some characteristic peaks of $H_{PAA-PAM}$ coating exhibited a slight shift compared with the $H_{PAA-PAM/Fe3+}$ substrate due to the absence of $-COO^{-}$-Fe^{3+} coordination (Figure S7). The hydrogel coating can grow not only on $H_{PAA-PAM/Fe3+}$ substrate but also on other Fe^{3+}-loaded substrates using carboxyl components, such as $H_{PNIPAM-PAA/Fe3+}$ (Figure S8) and $H_{PHEMA-PAA/Fe3+}$ (Figure S9) substrate, indicating that the UV-SCIRP method is applicable for all Fe^{3+}-loaded hydrogel substrates. After coating a new layer of hydrogel through the UV-SCIRP method, the surface physicochemical properties of the original hydrogel substrates, including wettability and lubrication, can be altered significantly. In a typical case, the static contact angle of water droplets on bare $H_{PAA-PAM/Fe3+}$ substrate was about 87.1°, while it reduced to 20.3° and 67.7° after growing new $H_{PAA-PAM}$ and $H_{PNIPAM-PAA}$ coatings, respectively (Figure 2H). Similarly, the friction coefficient also changed from 1.24 to 0.06 and 0.03 for the said coatings, respectively (Figure 2I).

Continuous manufacture of multi-layered hydrogel structure

Similar to natural tissues, the layered structure of multi-layered hydrogel materials can endow each layer with specific physical or chemical properties to make the materials multi-functional. Even though the fabrication of multi-layered hydrogel

materials has always been a substantial challenge,[31] it is possible to successfully engineer multi-layered structural hydrogel materials with tunable layer components and reasonable interface bonding strength through the reiterative UV-SCIRP process. Figure 3A illustrates the schematic diagram for continuously growing multi-layered $H_{PAA\text{-}PAM/Fe3+(i\ =\ n)}$ materials by the UV-SCIRP method. The cross-sectional optical microscope photograph of the layered $H_{PAA\text{-}PAM/Fe3+(i\ =\ 6)}$ material with six layers is shown in Figure 3B. The hydrogel shows apparent layered structure and uniform hydrogel thickness of ~120 μm for each layer. By and large, the total thickness reached 1,250 μm after nine cycles of the UV-SCIRP process (Figure 3C), and in principle the thickness could indefinitely increase with more cycles of UV-SCIRP. The scanning electron microscopy (SEM) images revealed that interfaces between the substrate hydrogel and the first hydrogel layer (i = 1) (Figure 3D) or among the other layers (i = 5 and i = 6) (Figure S10) were all seamlessly combined. The interface bonding forces were quantitatively characterized through a 180° peeling test. As shown in Figure S11, the average bonding force between the original substrate hydrogel and the first hydrogel layer was about 300 N/m, while it was about 150 N/m between the fifth and the sixth layer. Such good bonding force can be attributed to the interpenetrated polymer chains at the interface of the hydrogel layer network. As a comparison, a thick $H_{PAA\text{-}PAM}$ layer was generated on the surface of bulk $H_{PAA\text{-}PAM/Fe3+}$ substrate by pouring monomer solution and performing a traditional radical polymerization method (60°C for 2 h). The interface bonding force between $H_{PAA\text{-}PAM}$ layer and $H_{PAA\text{-}PAM/Fe3+}$ substrate was only about 0.15 N/m, and the hydrogel layer was prone to delaminate in the process of bending (Figure S12).

On a more essential note, multi-layered hydrogels with alternating components and tunable thickness were successfully fabricated by implementing the UV-SCIRP method using different monomer solutions (Figure 3E). Figure 3F illustrates the cross-sectional microscope photographs of the as-prepared three-layered $H_{(PAA\text{-}PAM/Fe3+)\&(PNIPAM\text{-}PAA/Fe3+)\&(PAA\text{-}PAM/Fe3+)}$ material with both high strength and high stimulus responsiveness (the middle $H_{PNIPAM\text{-}PAA/Fe3+}$ layer is the temperature-responsive layer) in 20°C and 40°C water baths. Upon immersion into the 40°C water bath, the thickness of the $H_{PNIPAM\text{-}PAA/Fe3+}$ layer showed an evident decrease due to the conformation transition of poly(N-isopropylacrylamide) (PNIPAM) chains from coil (hydrophilic state) to globule state (hydrophobic state).[56] Likewise, the dynamic evolution of the network structure for the middle layer can be intuitively verified by monitoring the transmittance change of the whole material. As shown in Figure 3G, a photograph of the *Mona Lisa* underneath a three-layered $H_{(PAA\text{-}PAM/Fe3+)\&(PNIPAM\text{-}PAA/Fe3+)\&(PAA\text{-}PAM/Fe3+)}$ material could reversibly appear and disappear, upon heating it to 40°C and then cooling it to 20°C (Video S1), indicating that the spatial responsiveness of an entire layered hydrogel material can be precisely controlled by phase change of a specific inner layer network. This implies that the layered structural hydrogels with integrated dual functionality or multi-functionality could be achievable via multiple cycles of the UV-SCIRP process with different functionality-yielding monomer solutions. In addition, smart layered soft actuators can be developed upon growing responsive $H_{PNIPAM\text{-}PAA/Fe3+}$ coatings on the surface of $H_{PAA\text{-}PAM/Fe3+}$ substrates. As shown in Figure S13, the layered hydrogel can curve as a tube after being immersed in a 40°C water bath for 13 s (Video S2), signifying its promising application in the field of soft actuation devices.

The construction of patterned, gradient, and complex layered structural hydrogels

Furthermore, the UV-SCIRP method can also be selectively applied to localized regions in order to create patterned or gradient layered hydrogel materials, with the

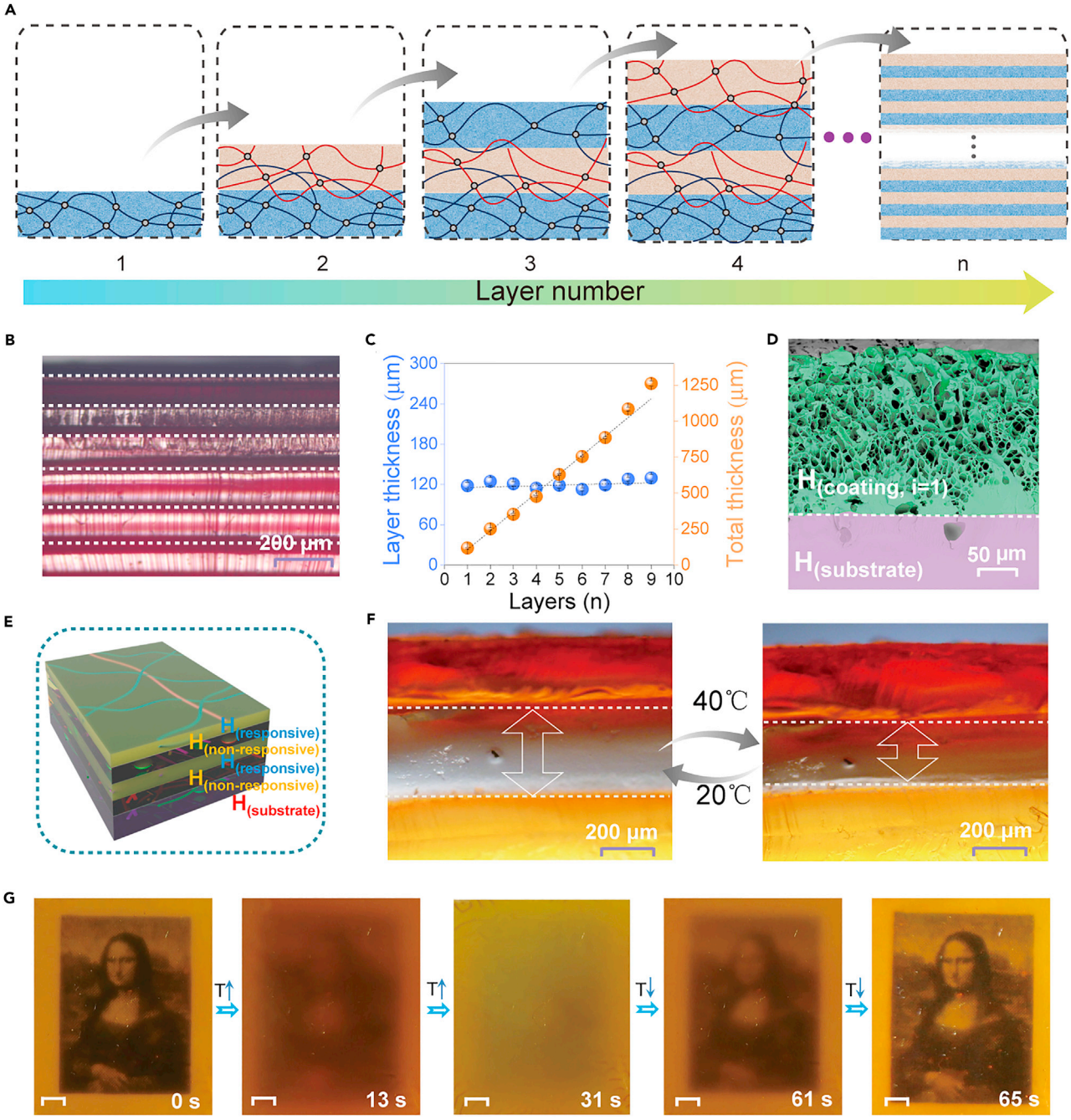

Figure 3. Continuously growing multi-layered hydrogel structure and spatial control of inner network layer

(A) A schematic diagram of multi-layered $H_{PAA\text{-}PAM/Fe3+(i\ =\ n)}$ material prepared by performing UV-SCIRP repetitively.

(B) A cross-sectional optical microscope photograph of layered $H_{PAA\text{-}PAM/Fe3+(i\ =\ 6)}$ material with six layers.

(C) The change of total layers thickness versus layer number and each layer thickness. The data are presented as mean ± SD and sample size n = 5.

(D) An SEM image showing the cross-sectional morphology at the interface between $H_{PAA\text{-}PAM/Fe3+}$ substrate and the first $H_{PAA\text{-}PAM}$ layer.

(E) A schematic diagram of multi-layered hydrogel material with alternating components and responsive behavior.

(F) Cross-sectional optical microscope images showing the thickness changes of the as-prepared three-layered $H_{(PAA\text{-}PAM/Fe3+)\&(PNIPAM\text{-}PAA/Fe3+)\&(PAA\text{-}PAM/Fe3+)}$ material upon immersing it in 20°C and 40°C water baths.

(G) Snapshots of a photograph of the *Mona Lisa* below the three-layered $H_{(PAA\text{-}PAM/Fe3+)\&(PNIPAM\text{-}PAA/Fe3+)\&(PAA\text{-}PAM/Fe3+)}$ sheet upon heating to 40°C and subsequent cooling to 20°C (the scale bar, 2 mm).

assistance of a UV gray-scale exposure technique.[57] As shown in Figure 4A, the China map is evidently visible after irradiating the $H_{PAA\text{-}PAM/Fe3+}$ substrate with a Digital Light Processing (DLP) UV projector due to the spatial control of generation of the Fe^{2+} ion catalyst on the hydrogel substrate. The same China map appeared green after treating the $H_{PAA\text{-}PAM}$ coating with fast green FCF for 1 min. Utilizing the UV-SCIRP method, several patterned $H_{PAA\text{-}PAM}$ coatings with diverse styles, including round dots and English and Chinese letters, can be easily produced (Figure 4B). In addition, it is also possible to grow a thermo-sensitive patterned $H_{PNIPAM\text{-}PAA}$ coating into desired patterns on the surface of an $H_{PAA\text{-}PAM/Fe3+}$ substrate. For example, the thermo-sensitive logo of the Lanzhou Institute of Chemical Physics (LICP) can be successfully made with an $H_{PNIPAM\text{-}PAA}$ coating, which appeared quite misty in a 20°C water bath, but became clear in a 40°C water bath due to the phase transition of PNIPAM chains (Figure 4C). More importantly, the $H_{PAA\text{-}PAM}$ coating with gradient layer thickness can also grow efficaciously due to the gradient distribution of Fe^{2+} ions as a result of gradient exposure from left to right (Figures 4D and S14). Interestingly, the current UV-SCIRP method not only allows the generation of hydrogel coatings on a flat substrate, but also can cater to various curved, spherical, and tubular surfaces (Figure 4E). In a typical case, $H_{PAA\text{-}PAM}$ coating can be easily generated on the surface of conical (Figure $4E_1$; layer thickness: 221 μm) and spherical (Figure S15; layer thickness: 296 μm) $H_{PAA\text{-}PAM/Fe3+}$ objects. Furthermore, both the outer and the inner surface of the nine channels of the complex hydrogel structure can be uniformly covered by a continuous layer of $H_{PAA\text{-}PAM}$ coating (layer thickness: 337 μm) through the UV-SCIRP method (Figure $4E_2$), indicating the possible application of this object as a fluid device. Finally, the scalability of the current method for complex and micro-3D hydrogel structures was examined. Microgels are typically spherical micrometer-scale polymer gel particles with intramolecular cross-linking structures,[58] and it is a major challenge to grow hydrogel coatings on their surface. This UV-SCIRP method has been utilized to generate a uniform hydrogel layer on the surface of the spherical microgels (Figure 4F). Compared with the bare PAA-PAM/Fe^{3+} microgels, whose surfaces tend to be very smooth and compact (Figure 4G), all of the samples, even with variable sizes, were uniformly wrapped by $H_{PAA\text{-}PAM}$ coating after the UV-SCIRP method was performed on them (Figure 4H). The cross-sectional morphology of spherical $H_{PAA\text{-}PAM}$ coating shells, after removing the PAA-PAM/Fe^{3+} microgel core (Figure 4I), further validated the successful furnishing of microgels.

Preparation of blood vessel-like diverse layered hydrogel tubes

The current method is also suitable for engineering blood vessel-like multi-layered hydrogel structures. The artery wall, for example, is a naturally layered tissue and includes the tunica externa, tunica medium, and tunica intima (Figure 5A). Figure 5B demonstrates a two-layered $H_{(PAA\text{-}PAM/Fe3+)\&(PAA\text{-}PAM)}$ tube, with an evident layered structure along with seamless interfacial bonding between the dense $H_{PAA\text{-}PAM/Fe3+}$ substrate layer and the porous $H_{PAA\text{-}PAM}$ layer (Figure 5C). Compared with a pure lubricious single network $H_{PAA\text{-}PAM}$ tube and a high-strength double-cross-linked $H_{PAA\text{-}PAM/Fe3+}$ tube, the two-layered $H_{(PAA\text{-}PAM/Fe3+)\&(PAA\text{-}PAM)}$ tube manufactured using the UV-SCIRP method exhibited both high strength (Figure S16) and low friction (Figure S17) features. In the same manner, a seven-layered $H_{PAA\text{-}PAM/Fe3+}$ tube with an apparent layered structure and uniform layer thickness was also facilely prepared (Figure 5D), with a total tube wall thickness from about 267 to 1,219 μm with an increasing number of layers (Figure 5E). The cross-sectional SEM image demonstrates the efficacious formation of a compact and interpenetrated network at the interface among these layers (Figure 5F). Furthermore, the layered hydrogel tube with alternative components and network structure can also be achieved by

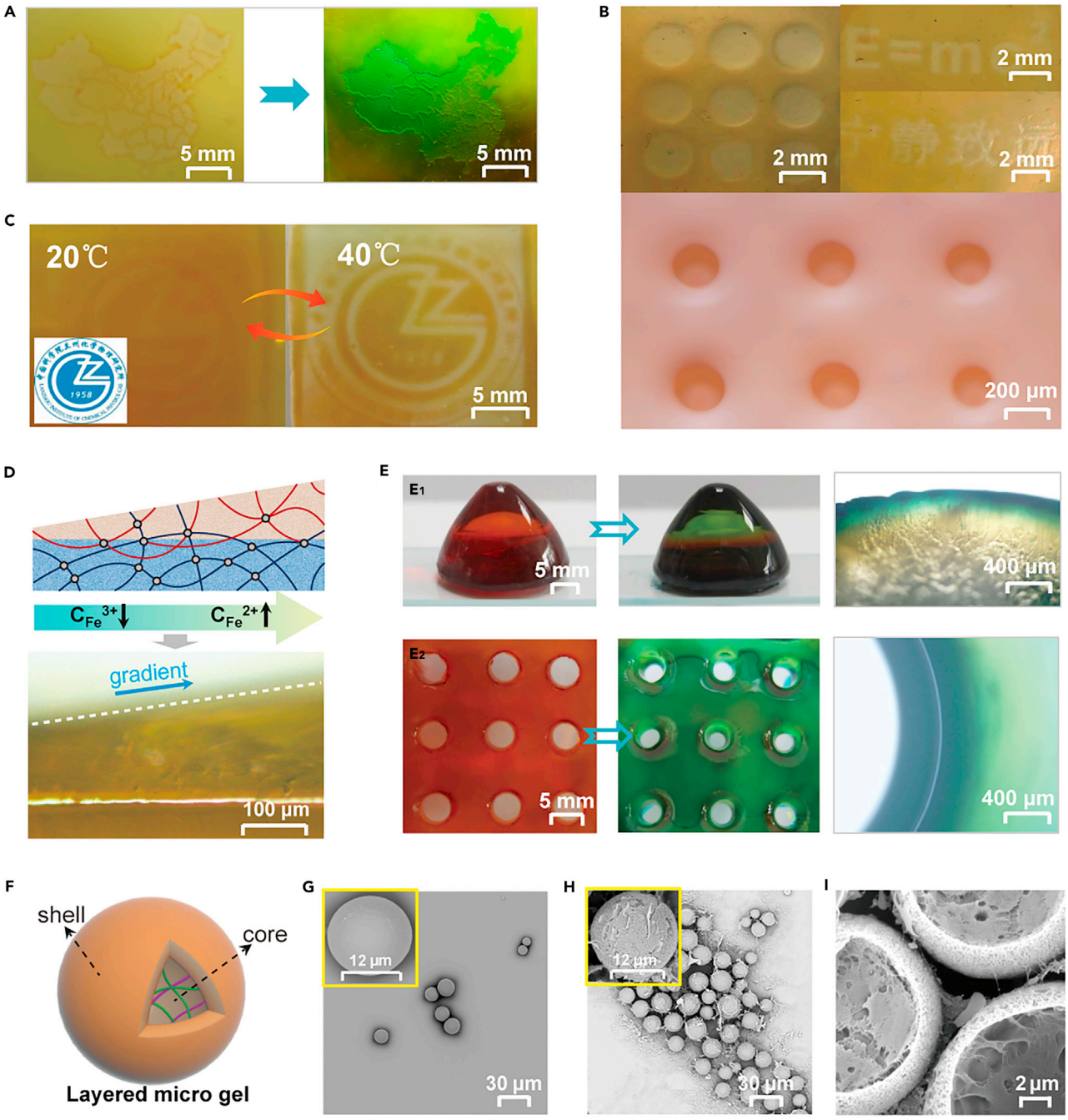

Figure 4. Various patterned, gradient, and complex layered structural hydrogels created by the UV-SCIRP method

(A) A map of China generated on the surface of an $H_{PAA\text{-}PAM/Fe3+}$ substrate with the assistance of a UV gray-scale exposure technique (left) and after growing an $H_{PAA\text{-}PAM}$ coating by the UV-SCIRP method for 1 min (right, dyed with fast green FCF).

(B) Different patterned $H_{PAA\text{-}PAM}$ coatings, including round dots and English and Chinese letters, produced by the UV-SCIRP method.

(C) The color change of a patterned $H_{PNIPAM\text{-}PAA}$ coating (growth time: 30 s) showing the sign of Lanzhou Institute of Chemical Physics (LICP), in 20°C and 40°C water baths.

(D) A schematic diagram (top) and a microscope image (down) of an $H_{PAA\text{-}PAM/Fe3+}$ substrate with gradient $H_{PAA\text{-}PAM}$ coating (growth time: 1 min).

(E) Photographs and cross-sectional optical images showing the growth of an $H_{PAA\text{-}PAM}$ coating on the surface of a conical $H_{PAA\text{-}PAM/Fe3+}$ object (E_1) and $H_{PAA\text{-}PAM/Fe3+}$ block with nine channels (E_2).

(F) A schematic diagram showing the generation of a uniform $H_{PAA\text{-}PAM}$ coating on the surface of PAA-PAM/Fe^{3+} microgels.

Figure 4. *Continued*
(G) The surface morphology of PAA-PAM/Fe^{3+} microgels.
(H) The surface morphology of PAA-PAM/Fe^{3+} microgels after growing an $H_{PAA-PAM}$ coating for 4 min.
(I) The cross-sectional morphology of the spherical $H_{PAA-PAM}$ coating shell after removing the PAA-PAM/Fe^{3+} microgel core.

controlling the post-treatment time of the $H_{PAA-PAM}$ layer in the $FeCl_3 \cdot 6H_2O$ solution (Figure 5G), while the interface networks among these layers also appear closely interpenetrated (Figure S18). More importantly, the entire responsiveness of the as-prepared layered hydrogel tube can be reasonably controlled by integrating the responsive layer within the tube wall, which appears quite analogous to the expansion and contraction of a natural blood vessel under stimulation (by temperature, drug, etc.). For instance, a three-layered $H_{(PAA-PAM/Fe3+)\&(PNIPAM-PAA/Fe3+)\&(PAA-PAM/Fe3+)}$ tube with an intermediate responsive layer was prepared (Figures 5H and S19). Presumably, the total wall thickness of the three-layered hydrogel tube can be reversibly regulated upon alternating immersion in 20°C and 40°C water baths (Figure 5I). Meanwhile, the mechanical property of the three-layered hydrogel tube in the 40°C water bath was improved more obviously compared with that in the 20°C water bath (Figure S20). Furthermore, the current method can also be suitably applied for the manufacture of temperature-responsive layered complex hydrogel tube arrays by growing an $H_{PNIPAM-PAA}$ coating onto the outer surface of an $H_{PAA-PAM/Fe3+}$ tube array (Figure 5J). In particular, as a proof of concept for the prospective application of the three-layered responsive hydrogel tube (Figure 5K), a capillary containing rhodamine 6G (1 mg/mL) fluorescent dye was inserted into the channel of the tube (Figure 5L). In this setup, liquid dyes can be controlled in a reversible manner where they can disappear and appear on heating and cooling, indicating the potential functionality of this structure as a smart tubular fluid imaging device. Obviously, the precise control of mechanical properties and color evolution can be achieved by the fixed-point regional regulation of the internal spatial layer network for layered hydrogel tube materials.

Conclusions

In summary, a new interface polymerization method named UV-SCIRP for preparing layered structural hydrogels with a living polymerization growing process resembling the growth route of natural bio-tissues is reported in this paper. Fe^{2+} ions are produced *in situ* on the surface of the original Fe^{3+}-loaded hydrogel substrates through UV exposure reduction, where Fe^{2+} ions act as active catalysts so as to conduct radical polymerization at the solid-liquid interface, to generate uniform hydrogel coatings at room temperature. The polymerization mechanism was validated by employing the Fenton reaction and XPS spectrum analysis. The effects of some key factors dominating the amount of Fe^{2+} ion catalyst on the polymerization kinetics of the hydrogel layer were carefully evaluated. The current UV-SCIRP method appears suitable for the polymerization of multiple monomer solutions and can be positively utilized for effortlessly modifying surface wettability and lubricating properties. Multi-layered hydrogels can be prepared successfully via repetition of the UV-SCIRP method, and the components and network structures for each of its layers are feasibly controllable. The cross-sectional SEM characterizations demonstrate that the interface among these formed hydrogel layers was chemically interpenetrated; and the 180° peeling test results reveal the strong interface bonding force. Furthermore, layered hydrogel patterns with a certain designable shape can be achieved easily through assistance from the UV gray-scale exposure technique. Notably, the UV-SCIRP method can be suitably availed for diverse geometric surfaces of hydrogels, such as flat, curved, channel, and spherical geometries.

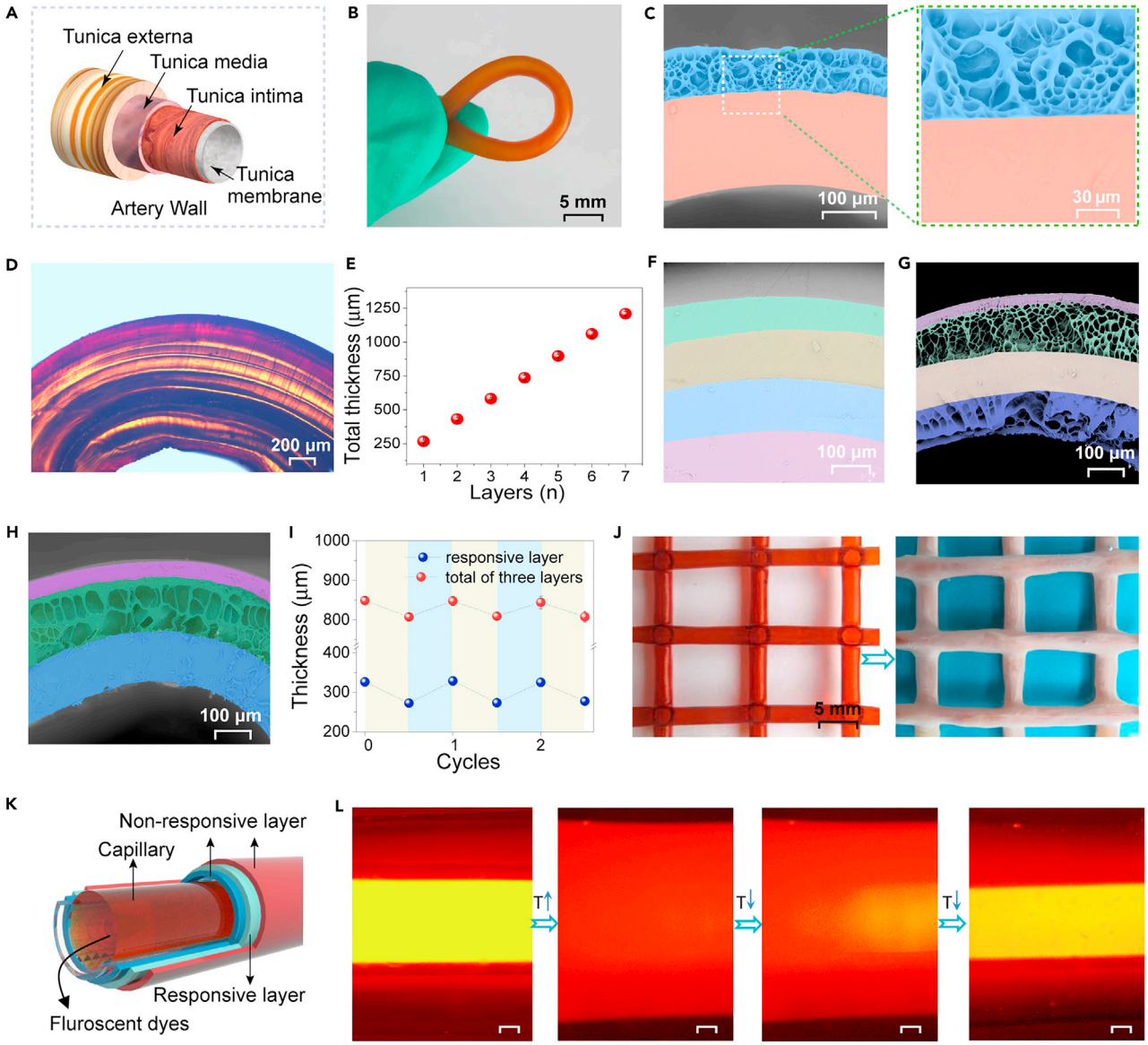

Figure 5. Preparation of blood vessel-like diverse layered hydrogel tubes

(A) A schematic diagram of the artery wall, which mainly includes three layers: tunica intima, tunica media, and tunica externa.

(B) Optical image of a two-layered $H_{PAA\text{-}PAM/Fe3+}$ tube.

(C) A cross-sectional SEM image of a two-layered $H_{(PAA\text{-}PAM/Fe3+)\&(PAA\text{-}PAM)}$ tube along with its local amplification (orange, the original $H_{PAA\text{-}PAM/Fe3+}$ tube wall layer; blue, the $H_{PAA\text{-}PAM}$ layer).

(D and E) An optical microscope image illustrating the cross-sectional wall of a seven-layered $H_{PAA\text{-}PAM/Fe3+}$ tube (D) and the total wall thickness versus layer number (E). The data in (E) are presented as mean ± SD and sample size n = 5.

(F) A cross-sectional SEM image showing the interface microstructure of the seven-layered $H_{PAA\text{-}PAM/Fe3+}$ tube from the fourth layer to the seventh layer (pink, fourth layer; blue, fifth layer, brown, sixth layer; green, seventh layer).

(G) A cross-sectional SEM image of a four-layered hydrogel tube with alternative components and network structure (purple, $H_{PAA\text{-}PAM}$ layer; gray, original $H_{PAA\text{-}PAM/Fe3+}$ tube wall layer; green, $H_{PAA\text{-}PAM}$ layer; pink, $H_{PAA\text{-}PAM/Fe3+}$ layer).

(H) A cross-sectional SEM image of a temperature-responsive three-layered $H_{(PAA\text{-}PAM/Fe3+)\&(PNIPAM\text{-}PAA/Fe3+)\&(PAA\text{-}PAM/Fe3+)}$ tube (blue, original $H_{PAA\text{-}PAM/Fe3+}$ tube wall layer; green, temperature-responsive $H_{PNIPAM\text{-}PAA/Fe3+}$ layer; pink, $H_{PAA\text{-}PAM/Fe3+}$ layer).

(I) The thickness change of the total tube wall and the responsive layer of the three-layered $H_{(PAA\text{-}PAM/Fe3+)\&(PNIPAM\text{-}PAA/Fe3+)\&(PAA\text{-}PAM/Fe3+)}$ tube (H) upon circularly immersing in 20°C and 40°C water baths. The data in (I) are presented as mean ± SD and sample size n = 5.

(J) Photographs showing the complex $H_{PAA\text{-}PAM/Fe3+}$ tube array (left) and after the growth of a responsive $H_{PNIPAM\text{-}PAA}$ coating on all the tubes' surface, after immersion in a 40°C water bath (right).

(K and L) A schematic diagram showing the insertion of a capillary containing rhodamine 6G (1 mg/mL) into the channel of a three-layered responsive $H_{(PAA\text{-}PAM/Fe3+)\&(PNIPAM\text{-}PAA/Fe3+)\&(PAA\text{-}PAM/Fe3+)}$ tube (K), and corresponding fluorescence snapshots over heating and cooling (scale bar, 200 μm) (L).

Meanwhile, a uniform hydrogel shell layer can be successfully grown on the surface of the spherical microgel core. It is demonstrated that blood vessel-like multi-layered hydrogel structures are feasible to manufacture. The current method offers a novel approach for developing bioinspired layered hydrogel structures that are suitable for a wide range of applications.

EXPERIMENTAL PROCEDURES

Resource availability

Lead contact

Further information and requests for resources and reagents should be directed to and will be fulfilled by the lead contact, Shuanhong Ma (mashuanhong@licp.cas.cn).

Materials availability

The following reagents used in this study were purchased from the indicated companies: acrylamide (AM; 99%, J&K Chemical Ltd.), acrylic acid (AA; >99%, TCI Co. Ltd.), MBAA (99%, Sigma-Aldrich), APS (≥98%, Chengdu Kelong Chemical Reagent Co. Ltd.), iron(III) chloride hexahydrate ($FeCl_3 \cdot 6H_2O$, AR, Tianjin Kemiou Chemical Reagent Co. Ltd.), citric acid monohydrate (AR, Chengdu Kelong Chemical Reagent Co. Ltd.), sodium hydroxide (NaOH, ≥96.0%, Tianjin Li'Anlong Bohua Pharmaceutical Chemistry Reagent Co. Ltd.), XO (AR, Tianjin Damao Chemical Reagent Factory), rhodamine 6G (98.5%, J&K Chemical Ltd.), 2-hydroxyethyl methacrylate (HEMA; 99%, J&K Chemical Ltd.), N-isopropylacrylamide (NIPAM; 98%, TCI Co. Ltd.), fast green FCF (high-purity grade, Solarbio), N,N,N′,N″,N″-pentamethyldiethylenetriamine (11,477, 98%, J&K Chemical Ltd.), Span 80 (CP, Heowns), Tween 80 (CP, Tianjin Third Chemical Reagent Factory), and iron(II) chloride tetrahydrate ($FeCl_2 \cdot 4H_2O$; AR, Xilong Chemical Co. Ltd.).

Data and code availability

All data needed to evaluate the conclusions in the paper are present in the paper and/or in the supplemental information. Additional data related to this paper may be requested from the authors.

The preparation of $H_{PAA\text{-}PAM/Fe3+}$ substrate

The chemically cross-linked $H_{PAA\text{-}PAM}$ substrate was prepared through free radical thermal polymerization. The preparation process was as follows: first, 4.26 g AM, 1.08 g AA, 0.0534 g APS, and 0.00864 g MBAA were dissolved in 30 mL deionized water (solution A), and then the above solution was degassed with N_2 for 10 min. Second, the solution was poured into the mold (glass plane used as two contact surfaces) with a thickness of 1 mm and put in an oven at 60°C for 2 h, for polymerization. After that, the chemically cross-linked $H_{PAA\text{-}PAM}$ substrate was immersed in 0.0162 g/mL $FeCl_3 \cdot 6H_2O$ solution for 12 h to form the secondary network. Finally, the prepared hydrogel was immersed in deionized water for 12 h to remove any free monomers and ferric ions, to obtain the final desired $H_{PAA\text{-}PAM/Fe3+}$ substrate.

The preparation of $H_{PHEMA\text{-}PAA/Fe3+}$ substrate

The chemically cross-linked $H_{PHEMA\text{-}PAA}$ substrate was prepared through free radical polymerization at room temperature. The preparation process was as follows: first, 7.80 g HEMA, 1.08 g AA, 0.0534 g APS, and 0.1728 g MBAA were dissolved in 40 mL deionized water; then this solution was degassed with N_2 for 10 min and then 40 μL accelerator 11,477 was added to the solution. Second, the solution was poured into the mold (glass plane used as two contact surfaces) with a thickness of 1 mm and placed at room temperature for 4 h for polymerization. Subsequently, the chemically cross-linked $H_{PHEMA\text{-}PAA}$ substrate was immersed in 0.0162 g/mL

$FeCl_3 \cdot 6H_2O$ solution for 12 h to form the secondary network. Finally, the prepared hydrogel was immersed in deionized water for 12 h to remove any free monomers and ferric ions, to obtain the final desired $H_{PHEMA\text{-}PAA/Fe3+}$ substrate.

The preparation of $H_{PNIPAM\text{-}PAA/Fe3+}$ substrate

The chemically cross-linked $H_{PNIPAM\text{-}PAA}$ substrate was prepared through free radical polymerization at room temperature. The preparation process was as follows: first, 6.78 g NIPAM, 0.864 g AA, 0.02 g APS, and 0.01 g MBAA (solution B) were dissolved in 40 mL deionized water; then this solution was degassed with N_2 for 10 min, and later, 40 μL accelerator 11,477 was added to the solution. Second, the solution was poured into the mold (glass plane used as two contact surfaces) with a thickness of 1 mm and placed at room temperature for 4 h for polymerization. Afterward, the chemically cross-linked $H_{PNIPAM\text{-}PAA}$ substrate was immersed in 0.0162 g/mL $FeCl_3 \cdot 6H_2O$ solution for 12 h to form the secondary network. Finally, the prepared hydrogel was immersed in deionized water for 12 h to remove any free monomers and ferric ions, to obtain the final desired $H_{PNIPAM\text{-}PAA/Fe3+}$ substrate.

The preparation of $H_{PAA\text{-}PAM/Fe3+}$ tubes

The $H_{PAA\text{-}PAM/Fe3+}$ tubes were prepared by the SCIRP method. The preparation process was as follows: first, a 3.0 mm iron wire was immersed in solution A after being degassed with N_2 for 10 min and polymerized for 5 min. Second, the hydrogel layer-wrapped iron wire was immersed in 0.0162 g/mL $FeCl_3 \cdot 6H_2O$ solution for 12 h. After that, it was soaked in deionized water for 12 h to remove any residual monomers and ferric ions. Finally, the iron wire was removed.

The preparation of an $H_{PAA\text{-}PAM/Fe3+}$ tube array

First, six iron wires (3.0 mm) were arranged in an orderly spaced 3D grid array, and solution A, after being degassed with N_2 for 10 min, was poured into the array to perform SCIRP for 5 min. Second, the array was immersed in 0.0162 g/mL $FeCl_3 \cdot 6H_2O$ solution for 12 h. Afterward, it was soaked in deionized water for 12 h, to remove any residual monomers and ferric ions. Finally, the iron wires were removed from the array.

The preparation of an $H_{PAA\text{-}PAM/Fe3+}$ block with nine channels

First, solution A, after being degassed with N_2 for 10 min, was poured into a square box glued with nine sequentially arranged cylinders, each having a diameter of 5 mm, and it was put in an oven at 60°C for 4 h for polymerization. Then, it was immersed in 0.0162 g/mL $FeCl_3 \cdot 6H_2O$ solution for 12 h; finally, it was immersed in deionized water for 12 h, to remove any free monomers and ferric ions.

The preparation of $H_{PAA\text{-}PAM/Fe3+}$ conical and spherical objects

First, solution A, after being degassed with N_2 for 10 min, was separately poured into molds, including conical and spherical-shaped molds, and placed in an oven at 60°C for 4 h for polymerization. After that, these objects, including conical and ball-shaped objects, were immersed in 0.0162 g/mL $FeCl_3 \cdot 6H_2O$ solution for 12 h to form the secondary network; finally, the hydrogel objects were immersed in deionized water for 12 h, to remove any free monomers and ferric ions.

The preparation of PAA-PAM/Fe^{3+} microgels

The PAA-PAM/Fe^{3+} microgels were successfully prepared by employing reverse-phase emulsion polymerization. The preparation details are as follows: 1.0 g Span 80 and 0.1 g Tween 80 were dissolved in 140 mL n-hexane and stirred mechanically at a speed of 350 rpm for half an hour, under the protection of N_2. After that, 1.6 g

AM, 0.4 g AA, 0.12 g MBAA, and 0.08 g APS were dissolved in 8 mL distilled water, and the mixed solution was added to the above solution dropwise while continuously stirring for 15 min. Finally, it was transferred to an oil bath at 60°C, to react for 4 h. The PAA-PAM microgels were obtained by centrifuging at a speed of 8,000 rpm for 5 min and then washing with deionized water and ethyl alcohol three times. After that, they were immersed in 0.0162 g/mL $FeCl_3 \cdot 6H_2O$ solution for 12 h; finally, they were immersed in deionized water to remove any free ferric ions, to get the desired PAA-PAM/Fe^{3+} microgels.

UV-SCIRP on Fe^{3+}-loaded hydrogel substrate surface to prepare layered hydrogels

First, 5.91 g citric acid monohydrate was dissolved in 150 mL deionized water, and 1 mol/L NaOH was added to this solution to adjust the pH level to 3.0. The Fe^{3+}-loaded hydrogel substrate prepared using the above method was immersed in the citric acid aqueous solution for a certain time. Then, the Fe^{3+}-loaded hydrogel materials were put into a customized transparent glass mold and exposed to UV light (365 nm, 15 mW/cm^2) for a few minutes to actuate the reduction of Fe^{3+} ions to Fe^{2+} ions. Meanwhile, the vertical free distance between glass mold and surface of Fe^{3+}-loaded hydrogel substrate was controlled at 0.5 cm to prevent the dehydration of the hydrogel and Fe^{2+} ion generation only on a superficial layer in the process of subsequent UV illumination. Finally, the hydrogel materials were immersed in the monomer solution to perform SCIRP, and a uniform hydrogel layer was seen forming on the surface of the hydrogel substrate after a certain reaction time. The UV-SCIRP recipes for monomer solutions for PAA-PAM and PNIPAM-PAA are as follows: 4.26 g AM, 1.08 g AA, 0.0534 g APS, 0.00864 g MBAA, and 30 mL H_2O (solution A); 6.78 g NIPAM, 0.864 g AA, 0.02 g APS, 0.01 g MBAA, and 40 mL H_2O (solution B).

UV-SCIRP on the surface of $H_{PAA\text{-}PAM/Fe3+}$ objects

Here, the above-mentioned process was repeated. The processing times were as follows: time in citric acid (conical objects, spherical objects, and hydrogel block with nine channels), 30 min; UV illumination time, 2 min; growth time, 2 min; and Fe^{3+} loading time, 12 h.

UV-SCIRP on the surface of PAA-PAM/Fe^{3+} microgels

First, 5.91 g citric acid monohydrate was dissolved in 150 mL deionized water, and 1 mol/L NaOH was added to this solution to adjust the pH level to 3.0. The PAA-PAM/Fe^{3+} microgels were then immersed in the above-mentioned citrate solution for 10 min, after which they were irradiated with UV light for 2 min and finally put in solution A for 4 min, to perform SCIRP.

The preparation of multi-layered $H_{PAA\text{-}PAM/Fe3+}$ materials by UV-SCIRP

First, 5.91 g citric acid monohydrate was dissolved in 150 mL deionized water, and 1 mol/L NaOH was added to this solution to adjust the pH level to 3.0. The $H_{PAA\text{-}PAM/Fe3+}$ substrate was immersed in the above-mentioned citric acid aqueous solution for 30 min. Second, the $H_{PAA\text{-}PAM/Fe3+}$ substrate was exposed to UV light for 2 min to trigger the reduction of Fe^{3+} ions to Fe^{2+} ions. Then, the $H_{PAA\text{-}PAM/Fe3+}$ substrate was immersed in solution A for 2 min, to perform SCIRP, and later soaked in 0.0162 g/mL $FeCl_3 \cdot 6H_2O$ solution for 12 h to form the secondary network. Finally, the hydrogel was immersed in deionized water for 12 h to remove any free monomers and ferric ions. The process was conducted repeatedly, which resulted in the successful preparation of the multi-layered $H_{PAA\text{-}PAM/Fe3+}$ materials.

The preparation of multi-layered $H_{(PAA\text{-}PAM/Fe3+)\&(PNIPAM\text{-}PAA/Fe3+)}$ materials by UV-SCIRP

The process is similar to the above-mentioned method of preparing multi-layered $H_{PAA\text{-}PAM/Fe3+}$ materials. The only difference is that the hydrogel material was alternatively immersed in solutions A and B, to perform SCIRP. First, the hydrogel substrates, after being irradiated with UV light, were immersed in solution A for 2 min, to perform SCIRP, and then, the hydrogel materials, after being irradiated with UV light, were immersed in solution B for 8 min, to perform SCIRP. The alternate process was repeated over and over again until the multi-layered $H_{(PAA\text{-}PAM/Fe3+)\&(PNIPAM\text{-}PAA/Fe3+)}$ materials were prepared successfully.

The preparation of two-layered $H_{(PAA\text{-}PAM/Fe3+)\&(PAA\text{-}PAM)}$ materials by pouring monomer solution and performing traditional radical polymerization

First, the $H_{PAA\text{-}PAM/Fe3+}$ substrate was prepared using the above-mentioned method of preparing $H_{PAA\text{-}PAM/Fe3+}$ substrate. Then, the $H_{PAA\text{-}PAM/Fe3+}$ substrate was put into a watch glass and solution A was poured on the surface of the $H_{PAA\text{-}PAM/Fe3+}$ substrate. Finally, it was put into an oven at 60°C for 2 h for polymerization to obtain the two-layered $H_{(PAA\text{-}PAM/Fe3+)\&(PAA\text{-}PAM)}$ materials.

Growing a patterned and gradient hydrogel coating on the $H_{PAA\text{-}PAM/Fe3+}$ substrate surface

First, 5.91 g citric acid monohydrate was dissolved in 150 mL deionized water, and 1 mol/L NaOH was added to the solution, to adjust the pH level to 3.0. The $H_{PAA\text{-}PAM/Fe3+}$ substrate was immersed in the above-mentioned citric acid aqueous solution for 30 min. Then, the hydrogel substrate was put under a DLP UV projector (the shadow area is 5.803 × 3.303 cm, the entire pixel is 1,920 × 1,080, and the dot resolution is ~30 μm) for 5 min. Finally, the hydrogel substrate was immersed in monomer solution to perform SCIRP.

Growing an $H_{PNIPAM\text{-}PAM}$ coating on the surface of an $H_{PAA\text{-}PAM/Fe3+}$ tube array

First, 5.91 g citric acid monohydrate was dissolved in 150 mL deionized water, and 1 mol/L NaOH was added to the solution, to adjust the pH level to 3.0. The $H_{PAA\text{-}PAM/Fe3+}$ tube array was immersed in the above-mentioned citric acid aqueous solution for 2 min. After that, the $H_{PAA\text{-}PAM/Fe3+}$ tube was exposed to UV light for 2 min to actuate the reduction of Fe^{3+} ions to Fe^{2+} ions. Finally, the $H_{PAA\text{-}PAM/Fe3+}$ tube was immersed in solution B for 3 min, to perform SCIRP.

The preparation of multi-layered $H_{PAA\text{-}PAM/Fe3+}$ tubes

First, 5.91 g citric acid monohydrate was dissolved in 150 mL deionized water and 1 mol/L NaOH was added to the solution, to adjust the pH level to 3.0. The $H_{PAA\text{-}PAM/Fe3+}$ tube was immersed in the above-mentioned citric acid aqueous solution for 2 min. Second, the $H_{PAA\text{-}PAM/Fe3+}$ tube was exposed to UV light for 2 min to activate the reduction of Fe^{3+} ions to Fe^{2+} ions. Then, the $H_{PAA\text{-}PAM/Fe3+}$ tube was immersed in solution A for 1 min, to perform SCIRP, and later immersed in 0.0162 g/mL $FeCl_3 \cdot 6H_2O$ solution for 1 h, to form the secondary network. Finally, the hydrogel tube material was immersed in deionized water for 1 h to remove any free monomers and ferric ions. The process was repeated until the multi-layered $H_{PAA\text{-}PAM/Fe3+}$ tube materials were prepared successfully.

The preparation of multi-layered $H_{(PAA\text{-}PAM/Fe3+)\&(PNIPAM\text{-}PAA/Fe3+)}$ tubes

The process is similar to the above-mentioned method of preparing multi-layered $H_{PAA\text{-}PAM/Fe3+}$ tubes. The only difference is that the hydrogel tube material was alternaely immersed in solution A and in solution B for performing SCIRP. First, the

hydrogel tube, after being irradiated with UV light, was immersed in solution A for 1 min, to perform SCIRP; then, the hydrogel materials, after being irradiated with UV light, were immersed in solution B for 3 min, to perform SCIRP. The alternate process was repeated until the desired layered $H_{(PAA\text{-}PAM/Fe3+)\&(PNIPAM\text{-}PAA/Fe3+)}$ materials were prepared successfully.

The preparation of $H_{PAA\text{-}PAM/Fe3+}$ materials with $H_{PNIPAM\text{-}PAA}$ coating actuator

The chemically cross-linked $H_{PAA\text{-}PAM}$ substrate materials were prepared as per the method of preparing $H_{PAA\text{-}PAM/Fe3+}$ substrate, with the only differences being that the immersing time for 0.0162 g/mL $FeCl_3 \cdot 6H_2O$ solution was 20 min and the thickness of the mold was 0.25 mm. The sample was then immersed in citrate acid solution for 5 min, followed by an exposure to UV light for 2 min; then, it was put in solution B for 2 min, to perform SCIRP; finally, it was immersed in 0.0162 g/mL $FeCl_3 \cdot 6H_2O$ solution for 10 min.

The preparation of $H_{PAA\text{-}PAM}$ substrate loaded with Fe^{2+} ions

First, solution A was degassed with N_2 for 10 min. Second, the solution was poured into the mold (glass plane used as two contact surfaces) with a thickness of 1 mm and put in an oven at 60°C for 2 h, for polymerization to obtain the $H_{PAA\text{-}PAM}$ substrate. Then, the substrate was dried in a freeze-drying machine for 12 h (SCIENTZ-10 N, Ningbo Scientz Biotechnology Co. Ltd.). Finally, the dried substrate was immersed into $FeCl_2$ solution (5 mg/mL) for 1 h to load Fe^{2+} ions.

Characterization

The morphology images were obtained through SEM (PhenomPro X, the Netherlands) at an accelerating voltage of 5 kV. An electrical universal material testing machine with a 500 N load cell (EZ-Test, Shimadzu) was utilized to perform a 180° peeling test at the speed of 100 mm/min. The transmittance was monitored by a UV-visible spectrophotometer (PerkinElmer Lambda 8100c). The static contact angles in the air were characterized using a DSA-100 optical contact angle meter (Krüss Company, Germany) at ambient temperature (25°C) with a droplet of 5 μL deionized water. The average contact angle was calculated on the sample at three different positions. A PerkinElmer transform infrared spectrometer (PerkinElmer, USA) was employed to evaluate the chemical composition with attenuated total reflection (ATR)-FTIR). The surface chemical composition was acquired by the implementation of XPS on an ESCALAB 250xi spectrometer (Thermo Fisher Scientific, USA) characterized with Al Kα radiation. The mechanical property of the sample was measured on an electrical universal material testing machine with a 500 N load cell (EZ-Test, Shimadzu) at the testing velocity of 100 mm/min.

Monitoring the growth kinetics of UV-SCIRP

An Olympus optical microscope was employed to monitor the growth kinetics of UV-SCIRP. Typically, the hydrogel materials were cut into pieces of 5 × 1 mm and were put on the slide, to measure the thickness of the hydrogel coating. When the growth time was controlled, the UV illumination time, Fe^{3+} loading time, and time in citric acid separately accounted for about 3 min, 12 h, and 30 min, respectively. When the UV illumination time was controlled, the growth time, Fe^{3+} loading time, and time in citric acid separately were 2 min, 12 h, and 30 min, respectively. When Fe^{3+} loading time was controlled, the UV illumination time, growth time, and time in citric acid separately were 3, 2, and 30 min, respectively. When the time in citric acid was controlled, the UV illumination time, growth time, and Fe^{3+} loading time were 3 min, 2 min, and 12 h, respectively. In most experiments, the UV illumination time was fixed at 2 or 3 min. A UV illumination time that is too long will lead to

excessive Fe^{3+} ions being reduced, which would produce a large number of catalysts, causing uncontrollable growth of the hydrogel coating, while a UV illumination time that is too short will result in an insufficient amount of catalysts, exhibiting a growth rate that is too slow. Based on this, we chose 2 min or 3 min as an optimum time period for catalyst reduction to achieve moderate growth rate.

Friction test

A conventional pin-on-desk reciprocating tribometer (CSM, Switzerland) was utilized to conduct the friction test under 0.2 N and 1 Hz for 300 s in a water bath. The poly(-dimethylsiloxane) (PDMS) and curing agents (mass ratio 10:1) were transformed into elastomeric PDMS hemispheres, with a diameter of 6 mm under incubation in a 60°C oven for 4 h and used as pins. Each sample was measured at least three times at different positions to get the average value.

SUPPLEMENTAL INFORMATION

Supplemental information can be found online at https://doi.org/10.1016/j.matt.2021.11.018.

ACKNOWLEDGMENTS

We gratefully acknowledge support from the National Science Foundation of China (22032006, 52075522, and 22072169), the Key Research Program of the Chinese Academy of Sciences (XDPB24), and the Youth Innovation Promotion Association (2019411). M.H., S.W., and X.H. are grateful for the NSF award 1724526, the ONR award N000141712117, and the AFOSR award FA9550-18-1-0449.

AUTHOR CONTRIBUTIONS

S.M. and F.Z. conceived the project idea. S.M. drafted the experimental protocol. R.X. carried out the experiments. S.M., M.H., S.W., and X.H. discussed the results and analyses. Y.Z. and L.Z. assisted in preparing the figures. B.Y. and M.C. supervised the work. R.X. and S.M. organized and wrote the manuscript. M.H., S.W., X.H., and F.Z. revised the manuscript. All the authors discussed the manuscript.

DECLARATION OF INTERESTS

The authors declare no competing interests.

Received: September 4, 2021
Revised: October 11, 2021
Accepted: November 15, 2021
Published: December 9, 2021

REFERENCES

1. Seliktar, D. (2012). Designing cell-compatible hydrogels for biomedical applications. Science *336*, 1124–1128.
2. Parhi, R. (2017). Cross-linked hydrogel for pharmaceutical applications: a review. Adv. Pharm. Bull. *7*, 515–530.
3. Liu, Y., He, W., Zhang, Z., and Lee, B.P. (2018). Recent developments in tough hydrogels for biomedical applications. Gels *4*, 46.
4. Wang, J., Lin, L., Cheng, Q., and Jiang, L. (2012). A strong bio-inspired layered PNIPAM-clay nanocomposite hydrogel. Angew. Chem. Int. Ed. *51*, 4676–4680.
5. Hua, M., and He, X. (2021). Soft-fiber-reinforced tough and fatigue resistant hydrogels. Matter *4*, 1755–1757.
6. Avissar, Y., Choi, J., DeSaix, J., Jurukovski, V., Wise, R., and Rye, C. (2018). Biology (OpenStax).
7. Gray, H. (1918). Anatomy of the Human Body (Lea & Febiger).
8. Ni Annaidh, A., Bruyere, K., Destrade, M., Gilchrist, M.D., Maurini, C., Ottenio, M., and Saccomandi, G. (2012). Automated estimation of collagen fibre dispersion in the dermis and its contribution to the anisotropic behaviour of skin. Ann. Biomed. Eng. *40*, 1666–1678.
9. James, R., Kesturu, G., Balian, G., and Chhabra, A.B. (2008). Tendon: biology, biomechanics, repair, growth factors, and evolving treatment options. J. Hand Surg. *33*, 102–112.
10. Burton, A.C. (1954). Relation of structure to function of the tissues of the wall of blood vessels. Physiol. Rev. *34*, 619–642.
11. Sophia Fox, A.J., Bedi, A., and Rodeo, S.A. (2009). The basic science of articular cartilage:

structure, composition, and function. Sports Health *1*, 461–468.

12. Ahn, A.C., and Kaptchuk, T.J. (2011). Spatial anisotropy analyses of subcutaneous tissue layer: potential insights into its biomechanical characteristics. J. Anat. *219*, 515–524.

13. O'Leary, L.E., Fallas, J.A., Bakota, E.L., Kang, M.K., and Hartgerink, J.D. (2011). Multi-hierarchical self-assembly of a collagen mimetic peptide from triple helix to nanofibre and hydrogel. Nat. Chem. *3*, 821–828.

14. Hu, Z., and Chen, G. (2014). Novel nanocomposite hydrogels consisting of layered double hydroxide with ultrahigh tensibility and hierarchical porous structure at low inorganic content. Adv. Mater. *26*, 5950–5956.

15. Liu, G., Ding, Z., Yuan, Q., Xie, H., and Gu, Z. (2018). Multi-layered hydrogels for biomedical applications. Front. Chem. *6*, 439.

16. Kim, D., Kim, H., Lee, E., Jin, K.S., and Yoon, J. (2016). Programmable volume phase transition of hydrogels achieved by large thermal hysteresis for static-motion bilayer actuators. Chem. Mater. *28*, 8807–8814.

17. Yao, C., Liu, Z., Yang, C., Wang, W., Ju, X.-J., Xie, R., and Chu, L.-Y. (2015). Poly(N-isopropylacrylamide)-clay nanocomposite hydrogels with responsive bending property as temperature-controlled manipulators. Adv. Funct. Mater. *25*, 2980–2991.

18. Shim, T.S., Kim, S.H., Heo, C.J., Jeon, H.C., and Yang, S.M. (2012). Controlled origami folding of hydrogel bilayers with sustained reversibility for robust microcarriers. Angew. Chem. Int. Ed. *51*, 1420–1423.

19. Liu, Z.S., and Calvert, P. (2000). Multilayer hydrogels as muscle-like actuators. Adv. Mater. *12*, 288–291.

20. Lin, P., Zhang, R., Wang, X., Cai, M., Yang, J., Yu, B., and Zhou, F. (2016). Articular cartilage inspired bilayer tough hydrogel prepared by interfacial modulated polymerization showing excellent combination of high load-bearing and low friction performance. ACS Macro Lett. *5*, 1191–1195.

21. Zhang, R., Lin, P., Yang, W., Cai, M., Yu, B., and Zhou, F. (2017). Simultaneous superior lubrication and high load bearing by the dynamic weak interaction of a lubricant with mechanically strong bilayer porous hydrogels. Polym. Chem. *8*, 7102–7107.

22. Li, W., Kang, J., Yuan, Y., Xiao, F., Yao, H., Liu, S., Lu, J., Wang, Y., Wang, Z., and Ren, L. (2016). Preparation and characterization of PVA-PEEK/PVA-β-TCP bilayered hydrogels for articular cartilage tissue repair. Compos. Sci. Technol. *128*, 58–64.

23. You, B., Li, Q., Dong, H., Huang, T., Cao, X., and Liao, H. (2018). Bilayered HA/CS/PEGDA hydrogel with good biocompatibility and self-healing property for potential application in osteochondral defect repair. J. Mater. Sci. Technol. *34*, 1016–1025.

24. Chen, X., Wu, W., Guo, Z., Xin, J., and Li, J. (2011). Controlled insulin release from glucose-sensitive self-assembled multilayer films based on 21-arm star polymer. Biomaterials *32*, 1759–1766.

25. Duan, J., Hou, R., Xiong, X., Wang, Y., Wang, Y., Fu, J., and Yu, Z. (2013). Versatile fabrication of arbitrarily shaped multi-membrane hydrogels suitable for biomedical applications. J. Mater. Chem. B *1*, 485–492.

26. Yan, K., Ding, F., Bentley, W.E., Deng, H., Du, Y., Payne, G.F., and Shi, X.W. (2014). Coding for hydrogel organization through signal guided self-assembly. Soft Matter *10*, 465–469.

27. Kim, B.S., Park, S.W., and Hammond, P.T. (2008). Hydrogen-bonding layer-by-layer-assembled biodegradable polymeric micelles as drug delivery vehicles from surfaces. ACS Nano *2*, 386–392.

28. Fujie, T., Matsutani, N., Kinoshita, M., Okamura, Y., Saito, A., and Takeoka, S. (2009). Adhesive, flexible, and robust polysaccharide nanosheets integrated for tissue-defect repair. Adv. Funct. Mater. *19*, 2560–2568.

29. Choi, J., Konno, T., Takai, M., and Ishihara, K. (2009). Smart controlled preparation of multilayered hydrogel for releasing bioactive molecules. Curr. Appl. Phys. *9*, e259–e262.

30. Li, B., Gao, Y., Feng, Y., Ma, B., Zhu, R., and Zhou, Y. (2011). Formation of concentric multilayers in a chitosan hydrogel inspired by Liesegang ring phenomena. J. Biomater. Sci. Polym. Ed. *22*, 2295–2304.

31. Ladet, S., David, L., and Domard, A. (2008). Multi-membrane hydrogels. Nature *452*, 76–79.

32. Ladet, S.G., Tahiri, K., Montembault, A.S., Domard, A.J., and Corvol, M.T. (2011). Multi-membrane chitosan hydrogels as chondrocytic cell bioreactors. Biomaterials *32*, 5354–5364.

33. He, M., Zhao, Y., Duan, J., Wang, Z., Chen, Y., and Zhang, L. (2014). Fast contact of solid-liquid interface created high strength multi-layered cellulose hydrogels with controllable size. ACS Appl. Mater. Interfaces *6*, 1872–1878.

34. Nie, J., Lu, W., Ma, J., Yang, L., Wang, Z., Qin, A., and Hu, Q. (2015). Orientation in multi-layer chitosan hydrogel: morphology, mechanism, and design principle. Sci. Rep. *5*, 7635.

35. Nguyen, L.H., Kudva, A.K., Saxena, N.S., and Roy, K. (2011). Engineering articular cartilage with spatially-varying matrix composition and mechanical properties from a single stem cell population using a multi-layered hydrogel. Biomaterials *32*, 6946–6952.

36. Hume, S.L., Hoyt, S.M., Walker, J.S., Sridhar, B.V., Ashley, J.F., Bowman, C.N., and Bryant, S.J. (2012). Alignment of multi-layered muscle cells within three-dimensional hydrogel macrochannels. Acta Biomater. *8*, 2193–2202.

37. Steinmetz, N.J., Aisenbrey, E.A., Westbrook, K.K., Qi, H.J., and Bryant, S.J. (2015). Mechanical loading regulates human MSC differentiation in a multi-layer hydrogel for osteochondral tissue engineering. Acta Biomater. *21*, 142–153.

38. Roh, D., Choi, W., Kim, J., Yu, H.-Y., Choi, N., and Cho, I.-J. (2018). Fabrication of multi-layered macroscopic hydrogel scaffold composed of multiple components by precise control of UV energy. Biochip J. *12*, 280–286.

39. Kidoaki, S., Kwon, I.K., and Matsuda, T. (2005). Mesoscopic spatial designs of nano- and microfiber meshes for tissue-engineering matrix and scaffold based on newly devised multilayering and mixing electrospinning techniques. Biomaterials *26*, 37–46.

40. Okuda, T., Tominaga, K., and Kidoaki, S. (2010). Time-programmed dual release formulation by multilayered drug-loaded nanofiber meshes. J. Control Release *143*, 258–264.

41. Yang, G., Lin, H., Rothrauff, B.B., Yu, S., and Tuan, R.S. (2016). Multilayered polycaprolactone/gelatin fiber-hydrogel composite for tendon tissue engineering. Acta Biomater. *35*, 68–76.

42. Shang, W., Liu, Y., Wan, W., Hu, C., Liu, Z., Wong, C.T., Fukuda, T., and Shen, Y. (2017). Hybrid 3D printing and electrodeposition approach for controllable 3D alginate hydrogel formation. Biofabrication *9*, 025032.

43. Mredha, M.T.I., Le, H.H., Cui, J., and Jeon, I. (2020). Double-hydrophobic-coating through quenching for hydrogels with strong resistance to both drying and swelling. Adv. Sci. *7*, 1903145.

44. Hu, Z., Zhang, X., and Li, Y. (1995). Synthesis and application of modulated polymer gels. Science *269*, 525–527.

45. Magdanz, V., Stoychev, G., Ionov, L., Sanchez, S., and Schmidt, O.G. (2014). Stimuli-responsive microjets with reconfigurable shape. Angew. Chem. Int. Ed. *126*, 2711–2715.

46. Zarket, B.C., and Raghavan, S.R. (2017). Onion-like multilayered polymer capsules synthesized by a bioinspired inside-out technique. Nat. Commun. *8*, 193.

47. Barbey, R., Lavanant, L., Paripovic, D., Schuwer, N., Sugnaux, C., Tugulu, S., and Klok, H.A. (2009). Polymer brushes via surface-initiated controlled radical polymerization: synthesis, characterization, properties, and applications. Chem. Rev. *109*, 5437–5527.

48. Huang, X., and Wirth, M.J. (1997). Surface-initiated radical polymerization on porous silica. Anal. Chem. *69*, 4577–4580.

49. Frahn, J. (1958). The photochemical decomposition of the citrate-ferric iron comples: a study of the reaction products by paper ionoporesis. Aust. J. Chem. *11*, 399–405.

50. Gao, Y., Wu, K., and Suo, Z. (2019). Photodetachable adhesion. Adv. Mater. *31*, e1806948.

51. Ma, S., Yan, C., Cai, M., Yang, J., Wang, X., Zhou, F., and Liu, W. (2018). Continuous surface polymerization via Fe(II)-mediated redox reaction for thick hydrogel coatings on versatile substrates. Adv. Mater. *30*, e1803371.

52. Bennett, J.H., Lee, E.H., Krizek, D.T., Olsen, R.A., and Brown, J.C. (2008). Photochemical reduction of iron. II. Plant related factors. J. Plant Nutr. *5*, 335–344.

53. Abrahamson, H.B., Rezvani, A.B., and Brushmiller, J.G. (1994). Photochemical and spectroscopic studies of complexes, of iron(III) with citric acid and other carboxylic acids. Inorg. Chim. Acta *226*, 117–127.

54. House, D.A. (1962). Kinetics and mechanism of oxidations by peroxydisulfate. Chem. Rev. *62*, 185–203.

55. Wolff, S.P. (1994). Ferrous ion oxidation in presence of ferric ion indicator xylenol orange for measurement of hydroperoxides. Method Enzymol. *233*, 182–189.

56. Chen, L., Liu, M., Lin, L., Zhang, T., Ma, J., Song, Y., and Jiang, L. (2010). Thermal-responsive hydrogel surface: tunable wettability and adhesion to oil at the water/solid interface. Soft Matter *6*, 2708.

57. Kuang, X., Wu, J., Chen, K., Zhao, Z., Ding, Z., Hu, F., Fang, D., and Qi, H.J. (2019). Grayscale digital light processing 3D printing for highly functionally graded materials. Sci. Adv. *5*, eaav5790.

58. Plamper, F.A., and Richtering, W. (2017). Functional microgels and microgel systems. Acc. Chem. Res. *50*, 131–140.